



# HHS Public Access

Author manuscript

Cell Rep. Author manuscript; available in PMC 2021 September 19.

Published in final edited form as:

Cell Rep. 2021 August 03; 36(5): 109488. doi:10.1016/j.celrep.2021.109488.

## Excess dietary carbohydrate affects mitochondrial integrity as observed in brown adipose tissue

Althea N. Waldhart<sup>1</sup>, Brejnev Muhire<sup>1</sup>, Ben Johnson<sup>1</sup>, Dean Pettinga<sup>1</sup>, Zachary B. Madaj<sup>1</sup>, Emily Wolfrum<sup>1</sup>, Holly Dykstra<sup>1</sup>, Vanessa Wegert<sup>1</sup>, J. Andrew Pospisilik<sup>1</sup>, Xianlin Han<sup>2,3</sup>, Ning Wu<sup>1,4,\*</sup>

<sup>1</sup>Van Andel Institute, Grand Rapids, MI 49503, USA

<sup>2</sup>Barshop Institute for Longevity and Aging Studies, UT Health San Antonio, San Antonio, TX 78229, USA

<sup>3</sup>Department of Medicine, UT Health San Antonio, San Antonio, TX 78229, USA

<sup>4</sup>Lead contact

### SUMMARY

Hyperglycemia affects over 400 million individuals worldwide. The detrimental health effects are well studied at the tissue level, but the *in vivo* effects at the organelle level are poorly understood. To establish such an *in vivo* model, we used mice lacking TXNIP, a negative regulator of glucose uptake. Examining mitochondrial function in brown adipose tissue, we find that TXNIP KO mice have a lower content of polyunsaturated fatty acids (PUFAs) in their membrane lipids, which affects mitochondrial integrity and electron transport chain efficiency and ultimately results in lower mitochondrial heat output. This phenotype can be rescued by a ketogenic diet, confirming the usefulness of this model and highlighting one facet of early cellular damage caused by excess glucose influx.

### Graphical Abstract

This is an open access article under the CC BY-NC-ND license (<http://creativecommons.org/licenses/by-nc-nd/4.0/>).

\*Correspondence: ning.wu@vai.org.

#### AUTHOR CONTRIBUTIONS

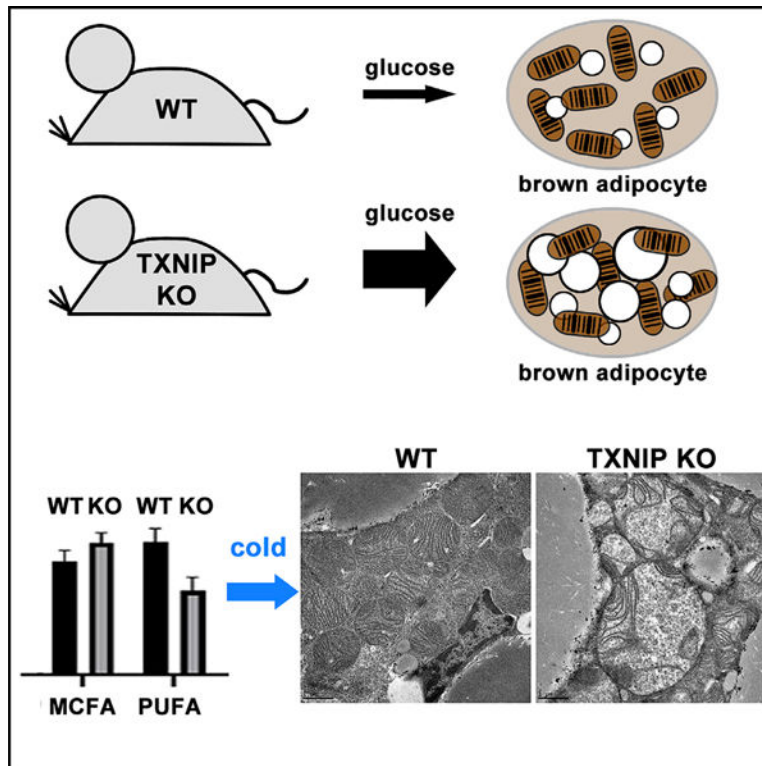
N.W. conceived the idea and designed and carried out most of the experiments with the help of A.N.W. Bioinformatics analysis was done by B.M., B.J., and D.P., and biostatistical analysis by Z.B.M. and E.W. H.D. did most of the qPCR analysis. The cardiolipin lipidomics was carried out in the Han laboratory.

#### SUPPLEMENTAL INFORMATION

Supplemental information can be found online at <https://doi.org/10.1016/j.celrep.2021.109488>.

#### DECLARATION OF INTERESTS

The authors declare no competing interests.



### In brief

Waldhart et al. show *in vivo* evidence that excess glucose has detrimental effects on mitochondrial function by changing the acyl-chain composition of structural lipids.

## INTRODUCTION

Glucose is a vital metabolite for human health. Accordingly, its blood concentration is tightly controlled. Dysregulation of glucose metabolism is a part of the clinical definition of diseases including metabolic syndrome and diabetes. Most agree that hyperglycemia eventually leads to insulin resistance once cells no longer take up glucose as directed. One can postulate that increased glucose influx causes dysfunction at the cellular level that ultimately results in insulin-unresponsive tissues. However, little is known about the nature of such cellular dysfunctions and the mechanisms that cause these changes.

To model an increase in cellular glucose uptake *in vivo* is not a trivial task. We took advantage of TXNIP (thioredoxin-interacting protein), a negative regulator of cellular glucose uptake. In its function as a regulator, TXNIP interacts with GLUT1, 2, 3, and 4 to facilitate their endocytosis via the clathrin-coated pathway (Waldhart et al., 2017; Wu et al., 2013). TXNIP additionally serves as a signaling node for cellular energy homeostasis. When cells need glucose—whether for energy-stressed cancer cells or during growth-factor-directed energy storage in muscle cells and adipocytes—TXNIP is phosphorylated and dissociates from GLUT1–4, allowing glucose influx. In the absence of TXNIP, the resulting uncontrolled intake of glucose causes hypoglycemia and hyperlipidemia in mice (Bodnar et

al., 2002; Sheth et al., 2005), but without the development of insulin resistance (Chutkow et al., 2008; Hui et al., 2004). Therefore, we reasoned that a TXNIP knockout (KO) would serve as a good starting model to improve our understanding of the *in vivo* effect of excess cellular glucose on mitochondrial function. To confirm the potential effects of glucose, we could employ a metabolic rescue, specifically a ketogenic diet, in which glucose availability would be systemically limited. Under such a diet, most cells would have to use fatty acids and ketone bodies for energy, thus neutralizing the effect of the TXNIP KO's unregulated glucose uptake.

Mitochondria, often referred to as the powerhouses of the cell, are highly studied organelles. Damaging mitochondria affects ATP production, metabolite conversion, and the production of cellular reactive oxygen species (ROS). Further, mitochondrial dysfunction is implicated in a variety of health issues including cardiovascular problems, neurodegeneration, and cancer.

Although we predicted that most organs would be adversely affected by elevated glucose intake, we focused on intrascapular brown adipose tissue (BAT) in this study for two reasons. First, brown adipocytes are dense with mitochondria and their thermogenic function entirely relies on mitochondrial integrity. Second, we could induce acute stress on BAT quite easily, via cold stress, to challenge their mitochondrial capacity. From our study, we discovered that excess glucose uptake into brown adipocytes led to fewer polyunsaturated fatty acids (PUFAs) in their cellular membranes. This alteration in fatty acid composition directly affected their mitochondrial integrity and functionality under stress conditions, resulting in reduced heat generation. This damaged mitochondrial phenotype was effectively rescued by a ketogenic diet, supporting our conjecture that elevated glucose intake is a primary reason for this dysfunction. In addition, we observed similar changes in cardiac tissue lipids, suggesting the inter-tissue lipid flux carries the change to non-lipogenic tissues. Altogether, these results support our prediction and provide direct evidence that cellular damage caused by excess carbohydrate intake is translated into mitochondrial membrane bilayer changes that affect cellular organelle function under stress.

## RESULTS

### TXNIP total KO brown adipose tissue has defective thermogenesis

We began our studies by comparing the morphology and marker gene expression of littermate-matched TXNIP wild-type (WT) and total KO BAT mice. Visually, KO BAT may appear paler than the WT BAT at room temperature (RT) (Figure 1A, top), reflecting the higher lipid content in KO brown adipocytes (Figure 1A, bottom). This was expected because the KO tissue takes in more glucose (Figure S1A; Parikh et al., 2007; Waldhart et al., 2017). To confirm whether BAT developed properly in KO animals, we checked marker gene expression, comparing WT and KO BAT to epididymal white adipose tissue (Figures 1B and S1B). The expression of the adipose marker *Adipoq* was similar in all these tissues, and neither the WT nor KO expressed the white adipose marker leptin. BAT-enriched markers (*Prdm16*, *Cidea*, *Ppara*, *Pdk4*, *Ucp1*, *Pgc1a*, *Dio2*, *Ebf3*, *Mpzl2*, and *Fbxo31*) all showed significantly higher gene expression in WT and KO BAT than in epididymal white

adipose tissue. However, the KO BAT had lower *Ucp1*, *Pgc1α*, and *Dio2* expression than the WT, indicating a possible thermogenic response issue.

We then tested whether KO BAT could be properly activated upon acute cold challenge by placing the mice at 4°C for 4 h. There was no visually dramatic difference between WT and KO (Figure 1C). Both the WT and KO BAT had lower lipid content due to the activation of fatty acid oxidation (Figures 1D and 1E). The cold stress induced acute gene transcription via cAMP and the phosphoCREB pathway. We measured mRNA from three early response genes—*Ucp1*; *Pgc1α*, an important co-activator for mitochondrial biogenesis (Puigserver et al., 1998); and *Dio2*—and found no differences after cold stress between WT and KO mice (Figure 1F). This meant that the KO BAT had a normal response to cold initially. To confirm our qPCR results, we ran western blots for UCP1 and PGC1α (Figures 1G and 1I). Even though there was no difference in PGC1α, there was less UCP1 protein both before and after cold stress in the KO, indicating multiple points for the regulation of UCP1, including basal gene transcription (different mRNA amount at RT), cold-responsive gene transcription (the same mRNA increase after cold), and translation (different protein amount both RT and cold).

Finally, we measured the surface temperature of the intrascapular BAT region during the 4°C cold stress using a thermocamera. These mice were not restrained during the experiment, so their body temperature was maintained in part by muscle shivering. As a control, there was no difference in temperature in the lumbar region between the WT and KO mice (Figure 1H, right). However, the intrascapular region of KO mice showed a lower temperature than did the WT (Figure 1H, left), indicating the KO BAT was generating less heat.

In conclusion, though many aspects of KO BAT appear as normal as those of the WT, KO BAT is less effective at heat generation, at least partly due to reduced UCP1, which is responsible for converting the mitochondrial proton gradient into heat.

### **TXNIP KO BAT mitochondria have defects that can be rescued with a ketogenic diet**

To examine whether the KO BAT heat deficit was solely due to less UCP1 protein, we examined mitochondrial integrity and the electron transport chain function. First, we used transmission electron microscopy (TEM) to see whether the mitochondria in the KO mice had structural defects. While there were no noticeable differences between the WT and KO mitochondria ultrastructure at RT (Figure 2A), after only a 4-h cold stress, the mitochondria of the KO animals were dramatically swollen and had broken cristae, a significant loss of structural integrity. To see whether the swollen phenotype was reversible, we moved the mice back to RT for 4 h after the cold stress; TEM showed a timely recovery of the mitochondrial ultrastructure in the KO mice (Figure 2B).

We next asked whether KO BAT mitochondria had difficulties catabolizing different types of metabolites. We isolated BAT mitochondria from WT and KO animals after a 4-h cold stress and carried out Seahorse oxygen consumption assays with three substrates: pyruvate/malate, glycerol-3-phosphate, or C16:0-carnitine (palmitoyl-carnitine)/malate (Figure 2C). Pyruvate is normally transported into the mitochondrial matrix by a voltage-dependent ion channel (VDAC) on the outer membrane and the mitochondrial pyruvate carrier on the

inner membrane (McCommis and Finck, 2015). Located on the outer surface of the inner mitochondrial membrane, mitochondrial glycerol-3-phosphate dehydrogenase directly uses coenzyme Q as the electron acceptor, so glycerol-3-phosphate needs to pass through VDAC (Mrá ek et al., 2013). Palmitoyl-carnitine is transported by CPT1A/B and SCL25A20 (Indiveri et al., 2011). We found that the oxygen consumption rate (OCR) was lower in the KO mice for all three substrates. Even after we used GDP to block UCP1 activity, we still observed lower electron transport chain activity with pyruvate and glycerol-3-phosphate. Given the various substrate types and alternative routes of utilization, this suggests that, in addition to the lower expression of UCP1, the electron transport chain, itself, is not operating efficiently in the KO mice.

To further support our conclusion that the observed impairments were the consequence of excess glucose uptake, we placed animals on a ketogenic diet. Since such a diet contains very little carbohydrate as well as fewer gluconeogenesis substrates (Table S1), whole-body energy metabolism is rerouted such that most tissues skew their macronutrient utilization away from glucose and toward fatty acids or ketone bodies. We hypothesized that a ketogenic diet would lessen the specific effects of glucose in TXNIP KO mice.

After keeping the animals on the ketogenic diet for 5 weeks, we first measured their BAT lipid content. There was no significant difference between the WT and KO BAT lipid content at either RT or after cold stress, although there was a decrease in triacylglycerides (TAG) after cold relative to RT (Figures 2D and S2A). When we checked the basal expression of *Ucp1*, *Pgc1a*, and *Dio2* at RT, there were no significant differences between WT and KO (Figure 2E); the rescue was also shown by western blots (Figures 2F and S2B). The decreased amounts of the ACLY1 and FASN proteins, as well as the increased blood ketone levels (Figure S2C), indicated that these mice were in ketosis.

Moreover, on the ketogenic diet, the KO mitochondrial ultrastructure after cold stress no longer showed a difference from the WT (Figure 2G). We subsequently isolated mitochondria from the mice on the ketogenic diet after cold stress and measured their OCR via Seahorse assays (Figure 2H). We saw similar OCRs between the WT and KO mitochondria, in contrast to the difference seen on the control diet. Altogether, these data demonstrate that a ketogenic diet was sufficient to rescue the mitochondrial structural and electron transport chain defects associated with TXNIP KO *in vivo*, and they highlight the profound ability of diet intervention to rescue specific genetic anomalies.

### **KO BAT showed lower expression of genes involved in PUFA transport and elongation**

In order to identify the cause of these mitochondrial defects, we carried out mRNA sequencing (mRNA-seq) on both WT and KO BAT before and after 4-h cold stress using the control diet or the ketogenic diet. Principal-component analysis showed that the samples clustered according to temperature in one dimension and diet in another dimension (Figure S3A), with all the triplicates clustering together. This was further supported by our Pearson correlation analysis (Figure S3B). We focused first on genes differentially expressed between WT and KO animals that were rescued by the ketogenic diet after cold stress. We identified 1,276 such genes, indicated in Figure 3A as red circles and listed in Table S2. We subsequently performed gene set enrichment analysis to test whether these genes

clustered in any of the predefined Gene Ontology (GO) pathways. Figure 3B shows both activated pathways (upregulated genes) and suppressed pathways (downregulated genes) in KO mice on the control diet that were rescued by the ketogenic diet. The most significantly rescued genes are involved in mitochondrial functions that were downregulated in KO mice on the control diet (Figure 3B). Thus, the bioinformatic analysis is in agreement with the experimental mitochondrial defects we observed after cold stress.

At RT, we identified 172 differentially expressed genes, 64 of which overlapped with the set of 1,276 (Figure 3C). Pathway analysis of the 172 genes did not show enrichment in mitochondria-related pathways. However, we did notice that the KO had reduced gene expression in multiple pathways involving verylong-chain fatty acid metabolism (Figure 3D). Many studies have shown that the mitochondrial inner membrane requires long-chain PUFAs, as well as a special form of lipid called cardiolipin, for generating the correct curvature and fluidity (Ikon and Ryan, 2017; Sustarsic et al., 2018). Optimal function of the electron transport chain depends on membrane lipid properties. We hypothesize that a disruption of PUFA supply in the KO mice leads to mitochondrial membrane lipid changes that manifest as the mitochondrial defects we observed after cold stress. Many of the longer PUFAs needed for membrane curvature, such as C22:6, can only be made from two essential dietary fatty acids, linoleic (C18:2[n-6]) and  $\alpha$ -linolenic (C18:3[n-3]) acids. A series of enzymes carry out elongation and desaturation reactions to make very long acyl chains (Figure S3C). Cardiolipin, a lipid with four acyl chains, is remodeled to include more PUFAs after its synthesis in the mitochondria. Therefore, we examined the gene expression in all fatty acid uptake, elongation, desaturation, and cardiolipin remodeling pathways that we know (not just the genes included in our pathway enrichment analysis). The relative expression changes of the genes in these pathways are shown in Figure 3E.

Even though we were looking for differentially expressed genes between WT and KO at RT, five genes stood out that exhibited a significant cold-induced expression increase: *Mfsd2A*, *Elovl 3*, *Elovl 4*, *Hacd2*, and *Lclat1*. MFSD2A is the sole lipid transporter known to specifically transport PUFAs (Nguyen et al., 2014; Wong et al., 2016); ELOVL3 and ELOVL4 carry out the first rate-limiting condensation step in fatty acid elongation (Ohno et al., 2010); HACD2 catalyzes the dehydration step; and LCLAT1 catalyzes the cardiolipin remodeling step. *Elovl 3*, *Elovl 4*, and *Hacd2* were included in the 172 RT gene set; *Mfad2A* and *Lclat1* were not included due to the statistical cut off we applied. Consistent with our hypothesis that the lipid composition of KO mitochondria might be dysregulated, these five genes all showed lower expression in the KO at RT as verified by qPCR (Figure 3F). More importantly, this difference at RT on the control diet was abolished by the ketogenic diet, consistent with the rescue by that diet (Figure 3G).

We also noticed (Figure 3E) that cold stress decreased the expression of *Scd2* and increased expression of *Fads3* (particularly in the KO) in the fatty acid desaturation pathway. SCD2 is a  $\Delta^9$  desaturase for C16:0 and C18:0. FADS3 is reported to generate a cis-double bond between C13-C14 (Karsai et al., 2020; Rioux et al., 2013). Neither of these genes is directly involved in PUFA synthesis, so we did not follow up further.

Two things are clear from our gene-expression study: (1) our comparison between the control and ketogenic diets suggests that insufficient long-chain PUFAs in the KO at RT contributes to the mitochondria's inability to increase flux under acute cold stress, consistent with both the TEM ultrastructure and oxygen consumption data; and (2) differences between the RT and cold gene expression indicate that BAT mitochondrial function has a high demand for long-chain PUFAs. The need to combat cold promotes increased fatty acid oxidation in BAT accompanied by lipid storage mobilization for catabolism. Opposite of this major direction of lipid flux, brown adipocytes separately uptake and elongate PUFAs specifically to meet the need for mitochondria in case the stress is prolonged and mitochondrial biogenesis is required.

To assess whether gene-expression changes are specifically occurring in the adipocytes in BAT, we generated adipocyte-specific TXNIP KO mice using AdipoQ-Cre (AKO) (Eguchi et al., 2011). Like the total KO animals, AKO mice showed a faster clearance of glucose (Figure S3D; Chutkow et al., 2008, 2010; Hui et al., 2004) and more fat mass, consistent with higher lipogenesis induced by glucose absorption (Figure S3E). We checked the mRNAs of *Elovl3*, *Elovl4*, and *Mfsd2a* in AKO mice and found the same results as in the total KOs (Figure S3F). We additionally confirmed similar phenotypes in mitochondria ultrastructure (Figure S3G) and oxygen consumption of isolated mitochondria in AKO (Figure S3H); both were rescued by the ketogenic diet. This confirmed that the PUFA uptake and elongation problems can be specific to the adipocytes lacking TXNIP, since adipocytes are lipogenic, converting excess glucose to lipids.

### KO BAT has less PUFA than WT BAT by lipidomics

To test whether the lipid metabolism gene-expression differences indeed affected lipid composition, we carried out lipidomics profiling of the WT and KO BAT from mice at RT. The dominant overall acyl-chain species in BAT were C14:0, C16:0, C16:1, C18:0, C18:1, and C18:2, and the major long-chain PUFA species was C22:6 (Figures 4A and S4A). All these acyl-chain variants can be synthesized *de novo* except for C18:2 and C22:6, which are predominantly obtained from diet. In agreement with the mRNA gene-expression data, KO BAT showed more medium-chain fatty acids (C14:0, C16:0, and C16:1), but much less C18:2. This is mirrored in TAG composition (Figure 4B), likely due to the high content of TAG in adipocytes. We then focused on the two major structural phospholipids in the cells: phosphatidylethanolamine (PE) and phosphatidylcholine (PC). While there was no major difference in PC between WT and KO (Figures 4C and S4B), we noticed significant difference in PE (Figures 4D and S4C). Compared with the total acyl-chain composition, PE had much higher content of PUFAs. The major species of PE contain C22:6, C20:4, and C18:2 at the sn2 position (Figure S4C). All PE species containing C22:6 were less abundant in KO mice than in the WT, while the C22:6 percentage content in PE was much higher than TAG (Figure 4D), indicating the importance of this long PUFA in maintaining structural membrane property. To obtain a better indication of mitochondrial-specific lipid profile effects, we analyzed the acyl chain composition of the isolated mitochondria only and saw the same trend of less C22:6 (Figure 4E).

Given the importance of the C22:6 contribution to membrane fluidity, the lipidomics results implied that the KO mitochondria had stiffer and less flexible mitochondrial membranes. This was consistent with the reversible mitochondria swelling we saw earlier, and it may contribute to the lower amount of UCP1 protein because UCP1 translation and function depends on membrane lipid properties (Hoang et al., 2013). To test whether there was a change in membrane fluidity due to the lipid profile changes, we used the lipophilic fluorescent probe Laurdan. Laurdan fluorescent emission is sensitive to its environment and is often used to provide information on the membrane fluidity and polarity (Harris et al., 2002; Parasassi et al., 1991). A high GP (general polarization) value is usually associated with low fluidity or low polarity of the membranes. As implied by the lipidomics data, mitochondria isolated from KO mice did have higher GP than those from WT (Figure 4F). At the same time, we saw the rescue of the difference by the ketogenic diet. In fact, the ketogenic diet has increased the mitochondrial membrane fluidity in both WT and KO mice compared to the aging diet. Further lipidomics analysis showed that mice on the ketogenic diet had increased C18:2 content relative to C18:1 in total lipids as well as in PE (Figures 4G–4J). Even though there was still a higher C22:6 amount in the WT in PE, the overall C22:6 dropped significantly in PE from >20% to ~10%, offset by increases in C18:2 and C20:4. These data support a lipid composition difference between WT and KO mitochondria that causes a functional difference in membrane properties, and this difference was rescued by a ketogenic diet.

Finally, even though we have shown that some of the defective mitochondrial properties hold true in adipose-specific TXNIP KO animals, this phenotype does not solely affect adipose tissue *in vivo*. Due to the inter-tissue lipid flux, we suspected that the shorter and more saturated acyl-chains synthesized from excess glucose are distributed throughout the body. To verify this, we performed lipidomics analysis of the heart, which is not known to carry out significant lipogenesis. We found the cardiac lipid content show the same trend as that of BAT. Although different lipid species have different relative contents of various acylchains, there was a general trend of less C22:6 in the KO, including cardiolipin (Figures 4K–4O; Figure S4D). mRNA-seq show no expression of Elov13 or MFSD2A, or any difference in other elongases between WT and KO in the heart. Therefore, it is likely the acyl-chain content difference in the heart comes from bulk lipid uptake from the blood.

The BAT and heart lipid profiles on different diets also highlight the complexity of how cells in different tissues sense and regulate the lipid acyl-chain composition in different classes of lipids in order to best achieve the bilayer properties needed for optimal function. Unexpectedly, instead of an increase the C22:6 content, BAT on the ketogenic diet decreased the use of C22:6, instead relying on the increase of C18:2 and C20:4. Similarly, the heart seemed to increase the use of C18:2 when there was less C22:6. We have not been able to detect any functional difference in cardiac mitochondria under basal conditions. We suspect that, like BAT, the heart needs to be put under metabolic stress in order to detect functional differences.

## DISCUSSION

Excess carbohydrate intake is implicated as one of the most common causes of metabolic duress that leads to diabetes and its complications. Dysfunctional mitochondria are thought to also play a key role in such metabolic problems. We are interested in identifying the early cellular changes using an *in vivo* model that links dietary carbohydrate intake to organelle function. We used TXNIP KO mice as a model for excess cellular glucose influx and used BAT thermogenesis as a measure of mitochondrial function. Further, we used a ketogenic diet as a nutrient rescue for reversing the effects of glucose.

We found that increased intracellular glucose availability directly influenced the function of the mitochondria by reducing membrane PUFA content. Under stress, this became detectable as deficiencies in mitochondrial electron transport chain function and structural integrity. While it is known that an increase in mitochondrial oxidative phosphorylation requires an influx of  $\text{Ca}^{2+}$  from the ER, we have not yet determined whether the reversible mitochondrial swelling in the KO mice was from the osmotic shock of  $\text{Ca}^{2+}$  influx or from the high electron potential generated across the inner mitochondrial membrane. Nevertheless, we found that membrane stability and flexibility were compromised. Another way to think about this stress treatment is that the detrimental effects of a high-carbohydrate diet on mitochondria likely accumulate early on, well before observable clinical symptoms. Such early deficiencies are difficult to detect in the absence of stress, yet they likely lay the foundation for subsequent chronic health issues. Given that the lipid changes affected total cellular lipids, we may reasonably infer that other organelle functions were affected as well. For example, there have been reports that ER function is affected by lipid composition (Rutkowski, 2019; Schroeder and Goh, 1980).

Given that diet affects the whole body, that *in vivo* regulation of glucose and lipids involves multiple organs and tissues, and that genetic variations among individuals are not likely restricted to any particular tissue, we performed most of our experiments using the complete knockout of TXNIP. We used adipose-specific knockouts to confirm that the effect of glucose on gene expression was still present when excess glucose uptake was restricted to adipocytes only. However, since adipose tissue is the major lipogenic site along with the liver, it is unsurprising that we captured the same phenotype as in the complete knockout. On the other hand, our lipid analysis on heart tissue indicated that the shifted acyl-chain distribution in the lipogenic tissues was passed to other tissues throughout the body by inter-tissue lipid flux. From these two tissues, we saw C22:6 was enriched in structural lipids relative to the TAG storage. However, a ketogenic diet seemed to reduce the demand for C22:6, since there was an increase supply of C18:2 as suggested by BAT PE data. It is still largely a mystery how cells sense membrane bilayer properties and determine what acyl-chains to incorporate, but it is clear that there is an optimal state the cells are trying to maintain.

Even though the ketogenic diet improved the mitochondrial response, it did not completely rescue all phenotypes of TXNIP KO, as indicated by all the gray circles in Figures 3A and 3C, as well as higher level of ACLY1 and FASN in KO mice (Figures 2F and S2B). This implies that even under the ketogenic condition, KOs are still carrying out lipogenesis.

Ketone bodies such as  $\beta$ -hydroxybutyrate (BHB) are not just fuel molecules, they are also signaling molecules activating G-protein-coupled receptors such as GPR43 (Miyamoto et al., 2019). In addition, BHB is an endogenous histone deacetylase inhibitor (Shimazu et al., 2013) with a protective role against oxidative stress. Therefore, it should be noted that a ketogenic diet produces other effects beyond minimizing glucose intake in cells. Furthermore, TXNIP has other roles, such as its association with inflammasomes (Lerner et al., 2012; Osowski et al., 2012; Zhou et al., 2010). Interestingly, the lipid composition change we showed here suggests that another way TXNIP can affect inflammation is via increased production of ROS from mitochondria with non-optimal membrane properties, although such minor changes in ROS would be difficult to detect *in vivo* with current technology.

From our study, there appear to be multiple means by which increased glucose uptake could affect lipid composition including (1) increased *de novo* lipid synthesis of medium-length and saturated fatty acids from glucose, (2) altered C18:2 and C18:3 absorption either in the intestine and/or in brown adipocytes themselves, and/or (3) reduced activity in acyl-chain elongation. The gene-expression differences after the cold treatment allowed us to identify some important genes for maintaining mitochondrial function at the basal state. The crucial question is, what transcription factors, influenced by cellular carbohydrates and lipids content, are responsible for the expression difference at the basal level? Several such factors are known. ChREBP/Mlx (Uyeda et al., 2002) and its homolog MondoA/Mlx (Stoltzman et al., 2008) are regulated by glucose-derived metabolites, while PPAR nuclear receptors are regulated by lipid species. *Elovl3*, *Mfsd2a*, and *Ucp1* are all reported to be PPAR-regulated genes (Berger et al., 2012; Jørgensen et al., 2007; Villarroya et al., 2007). Using the differentially expressed gene sets that we observed to be rescued by the ketogenic diet, we attempted to identify such transcription factors by motif enrichment analysis at the transcription start sites. Unfortunately, we were unable to identify any significant candidates, partly because some transcription factors (such as PPARs) prefer to bind at enhancers (Lefterova et al., 2008). One clear future direction would be to use chromatin immunoprecipitation sequencing (ChIP-seq) experiments to pinpoint the detailed mechanism and mutual regulation of metabolites and transcription.

Many cancer cells are known to upregulate glucose intake and carry out their own lipogenesis, generating sufficient lipid for membrane construction during replication (Röhrig and Schulze, 2016). Our results suggest that cancer cell mitochondria should have less oxidative phosphorylation activity due to having less PUFAs, which would partly explain their increased reliance on glycolysis for energy, forming a harmful negative-feedback loop. However, experiments to confirm this hypothesis were beyond the scope of our current study.

Ultimately, our findings illustrate a clear, early connection between excess carbohydrate and mitochondrial function *in vivo*. They confirm mechanistically one detrimental aspect of a high-sugar diet. While such cellular changes induced by diet may not be obvious under normal conditions, we provide strong evidence that they indeed make a functional difference under stress.

## STAR★METHODS

### RESOURCE AVAILABILITY

**Lead contact**—Further information and requests for resources and reagents should be directed to and will be fulfilled by the Lead Contact Ning Wu (ning.wu@vai.org).

**Materials availability**—This study did not generate new unique reagents.

**Data and code availability**—mRNaseq data generated during this study are available as PRJNA573103 and PRJNA681590 at BioProject.

There are no new codes generated for this study.

Any additional information required to reanalyze the data reported in this paper is available from the lead contact upon request.

### EXPERIMENTAL MODEL AND SUBJECT DETAILS

Mice were maintained in a barrier facility, in accord with the Institute's regulations for animal care and handling (IACUC 19–07-021). Strains TXNIPflox/flox (JAX 016847), CMV-Cre (JAX 006054), and Adipoq-Cre (JAX 028020) were purchased from the Jackson Laboratory. The total KO (CMV-Cre) mice were generated by crossing TXNIPflox/flox with CMV-cre mice. The Cre transgene was bred out during the process. The mice were backcrossed to C57B6/J (JAX 000664) or FVB (JAX 001800) for over 10 generations. The thermoimaging experiment was done on an FVB male background. The mRNA readout of gene expression was done on both the C57B6/J and the FVB background for both males and females; only the male C57B6/J data are shown. TEM, western blots, mitochondria Seahorse analysis, and lipidomics were done with C57B6/J males.

For experiments, sex-matched littermates between 2 and 3 months old were used. To cold-shock the mice, each mouse was placed in a paper bucket with some food, but no bedding, and then was placed in the cold room for indicated length of time (typically from 9 a.m. to 1 p.m.) before sacrifice by cervical dislocation.

### METHOD DETAILS

**Thermoimaging of mice**—Mice were placed individually in paper buckets with some food, but no bedding, and placed in the cold room. Thermoimages were taken at 0-, 2-, and 4-h time points using FLIR T250. For statistical analysis, the data were analyzed using linear mixed-effects models via the R v3.6.0 (<https://cran.r-project.org/>) package lme4. Random intercepts for each animal were included to account for repeated-measures, and Tukey HSD contrasts were used to test specific hypotheses while adjusting for multiple testing. The normality of residuals and random effects were verified visually via qq-plots.

**Mitochondria isolation and Seahorse analysis**—Intrascapular BAT was dissected out and minced on ice in isolation buffer (10 mM K-TES, pH 7.2, 250 mM sucrose, 2 mM taurine, 2% fatty acid-free BSA) plus protease inhibitors. The tissue with buffer was then homogenized in a Dounce homogenizer with pestle A 12 times and spun at  $800 \times g$  for 10

min at 4°C. The supernatant was passed through a 40-µm cell strainer and spun at 8000 × *g* for 10 min at 4°C. The pellet containing mitochondria was resuspended in buffer 2 (20 mM K-TES pH 7.2, 125 mM sucrose, 4 mM KH<sub>2</sub>PO<sub>4</sub>, 2 mM MgSO<sub>4</sub>, 1 mM EGTA) and the protein concentration was measured using Biorad Bradford assay. The mitochondria concentration was equalized among different samples, and the samples were then diluted in buffer 5 (20 mM K-TES pH 7.2, 125 mM sucrose, 4 mM KH<sub>2</sub>PO<sub>4</sub>, 2 mM MgSO<sub>4</sub>, and 0.1% fatty-acid free BSA) to the desired concentration for the Seahorse assay. The assay was carried out in buffer 5 with the addition of 4 mM ADP. The first addition in the assay was the substrates (5 mM pyruvate/6 mM malate (L/D mixture), or 10 mM glycerol-3-phosphate, or 4 µM palmitoyl-carnitine/4 mM malate (L/D mixture)). The second addition was 3 mM GDP to inhibit UCP1. The third addition was 2 µM oligomycin to inhibit ATP synthase and the fourth addition was 4 µM antimycin A.

**Membrane fluidity measurement with Laurdan**—Mitochondria were isolated as above. Laurdan was added at final 1 µM and incubated in the dark at 37°C for 30 min. The fluorescence was read in black 96-well plate on Biotek Synergy Neo2 Multi-mode Reader with excitation wavelength at 350 nm and emission wavelength at 435 nm and 500 nm. The general fluorescence was calculated as  $GP = (I_{435} - I_{500}) / (I_{435} + I_{500})$ .

**Transmission electron microscopy**—BAT tissue was dissected out and fixed in 2.5% glutaraldehyde and 2.5% paraformaldehyde in 0.1 M cacodylate buffer. Samples were sent to the Center for Advanced Microscopy at the Michigan State University, East Lansing, for analysis.

**Lipidomics**—The total lipid analysis on BAT from animals on the control diet was done by Metabolon Inc. (<https://www.metabolon.com/>). Isolated BAT tissue was snap-frozen in liquid nitrogen and shipped to Metabolon. The lipid amounts across samples were normalized according to the sample DNA concentration.

For other lipidomics, (including BAT mitochondrial lipids from control diet, BAT total lipids from ketogenic diet, and heart total lipids from control diet), tissues were snap-frozen in liquid nitrogen immediately after harvest and shipped to Prof. Han's laboratory at UT Health San Antonio. There, a small amount of tissue (about 10 mg) was homogenized in 0.5 mL of ice-cold diluted PBS (0.1 X) with a Potter-Elvehjem tissue grinder. Protein assay on an individual homogenate was conducted. An aliquot of homogenate was transferred to a disposable glass test tube. An internal standard (Tetra14:0 cardiolipin) for quantification of cardiolipin and lysoCL species was added to the tube based on the tissue protein content. Lipid extraction was performed using a modified procedure of Bligh and Dyer (Wang and Han, 2014). Cardiolipin and lysoCL species were analyzed by shotgun lipidomics as described previously (Han et al., 2006).

Lipidomics data in Figure S4 were analyzed using a beta mixed-effects model with a random effect for litter. When necessary, data were transformed according to previously documented methods to improve model fit (Smithson and Verkuilen, 2006).

**Western blots**—After treatment, mice were sacrificed by cervical dislocation and intrascapular BAT was dissected out and frozen immediately in liquid nitrogen and stored at  $-80^{\circ}\text{C}$ . Frozen tissues were lysed in RIPA buffer (30 mM Tris7.5, 120 mM NaCl, 1 mM vanadate, 20 mM NaF, 1% NP40, 1% deoxycholate, 0.1% SDS), plus protease inhibitors and calyculin A. The supernatant was used for running western blots.

**RNaseq and qPCR**—Total RNA was extracted with a PureLink RNA mini kit (Invitrogen12183018A) and submitted to the VAI genomics core. Libraries were prepared by the Van Andel Genomics Core from 500 ng of total RNA using the KAPA Stranded mRNA-Seq Kit (Roche). RNA was sheared to 200–300 bp. Prior to PCR amplification, cDNA fragments were ligated to Bioo Scientific NEXTflex DNA Barcodes (Bioo Scientific, Austin, TX, USA). The quality and quantity of the finished libraries were assessed using a combination of Agilent DNA High Sensitivity chip (Agilent Technologies, Inc.), QubitdsDNA HS Assay Kit (ThermoFisher Scientific, Waltham, MA), and Kapa Illumina Library Quantification qPCR assays (Kapa Biosystems). Individually indexed libraries were pooled and 75-bp, single-end sequencing was performed on an Illumina NextSeq 500 sequencer using a 75-bp HO sequencing kit (Illumina Inc., San Diego, CA, USA). Base calling was done by Illumina NextSeq Control Software (NCS) v2.0, and the output of NCS was demultiplexed and converted to FastQ format with Illumina Bcl2fastq v1.9.0.

For qPCR, total RNA was reverse-transcribed into cDNA using SuperScript IV Vilo Mastermix (Invitrogen). Primer sets used can be found in Table S3. For statistics, an unpaired Student's t test was performed using GraphPad Prism version 8.00 for Windows, GraphPad Software, La Jolla California USA

**Bioinformatics (RNA-seq data processing and analysis)**—Three biological replicates for each condition were sequenced and read mapping and differential expression analysis were performed using the RNA-seq pipeline implemented in snakePipe (Bhardwaj et al., 2019). Specifically, single-end reads were mapped to the mouse genome (mm10) using STAR aligner (Dobin et al., 2013) with default settings, reads mapped to genes were counted using featureCounts (Liao et al., 2014), and differential expression was done using DESeq2 (Love et al., 2014). The RPKM (reads per kilobase of transcript per million mapped reads) was computed using R from raw counts generated by SnakePipes RNA-seq pipelines. For quality control, samples and clustering of replicate performed principal component analysis on expression profiles using the prcomp function in R. A heatmap-based sample pairwise Person correlation coefficient and hierarchical clustering was generated with the pheatmap package in R.

The sets of differentially expressed genes between WT and KO whose differential expression was rescued by ketogenic diet – 1276 genes (cold) and 172 genes (RT) – were defined as genes that were significantly differentially expressed (with FRD  $< 0.05$ ) between WT and KO animals in the control diet but not significantly expressed in the ketogenic (FDR  $\geq 0.05$ ).

The heatmap comparing genes expression of all conditions relative to the RT/WT in five pathways (fatty acid uptake, elongation, desaturation, cardioliipin synthesis, and remodeling)

was generated using a ComplexHeatmap R package (Gu et al., 2016) based on log<sub>2</sub> CPM (Log<sub>2</sub> scaled count per million) values for all samples in triplicates, and each raw was mean-centered relative to the RT/WT mean.

Gene set enrichment analysis determines whether genes in predefined Gene Ontology gene sets are randomly distributed across the ranked list of differentially expressed genes or are preferentially found at the top or bottom. For both the RT and the cold samples, the GO-based methods were performed using gseGO functions implemented in the clusterProfiler R package (Subramanian et al., 2005; Yu et al., 2012). Sorted log<sub>2</sub> fold change expression values of differentially expressed genes were used as input. For gseGO, all subontology categories were used, and for significance a permutation test was set to 50,000, the minimum gene set size = 3, and maximum gene set size = 800.

**OGTT**—Male littermate matched *TXNIP<sup>fl/fl</sup>* and *AdipoQ-Cre Tg/+*, *TXNIP<sup>fl/fl</sup>* mice were fasted from 7 a.m. to 1:30 p.m. A bolus of glucose at 2 g/kg was delivered via oral gavage. Blood was sampled via the tail vein at various time points. OGTT data were analyzed using linear mixed-effects models via the R v3.6.0 (<https://cran.r-project.org/>) package “lme4.” Random intercepts for each littermate were included to account for repeated-measures. P values were multiple testing adjusted using Tukey HSD. Normality of residuals and random effects were visually assessed via qq-plots.

Lean mass and fat mass were measured with an EchoMRI-4n1–500 system. Bodyweight, lean mass, and fat mass data were analyzed using linear models via the R v3.6.0 (<https://cran.r-project.org/>) package “lme4.” P values were multiple testing adjusted using Tukey HSD. Normality of residuals were visually assessed via qq-plots.

Tissue TAG was measure with Infinity Triglyceride kit from ThermoFisher Scientific.

## QUANTIFICATION AND STATISTICAL ANALYSIS

Unless stated otherwise in Method details section (lipidomics), we assumed a normal distribution of the samples and Student’s t test (unpaired, two tailed) was used (Prism). The numbers of animals used (n), mean values and standard deviations (SD) were reported along the figure legends.

## Supplementary Material

Refer to Web version on PubMed Central for supplementary material.

## ACKNOWLEDGMENTS

The authors thank Alicia Withrow (Michigan State University) for TEM support. N.W. is supported by R01-GM120129. X.H. is partially supported by RF1 AG061872.

## REFERENCES

Berger JH, Charron MJ, and Silver DL (2012). Major facilitator superfamily domain-containing protein 2a (MFSD2A) has roles in body growth, motor function, and lipid metabolism. *PLoS ONE* 7, e50629. [PubMed: 23209793]

- Bhardwaj V, Heyne S, Sikora K, Rabbani L, Rauer M, Kilpert F, Richter AS, Ryan DP, and Manke T (2019). snakePipes: facilitating flexible, scalable and integrative epigenomic analysis. *Bioinformatics* 35, 4757–4759. [PubMed: 31134269]
- Bodnar JS, Chatterjee A, Castellani LW, Ross DA, Ohmen J, Cavalcoli J, Wu C, Dains KM, Catanese J, Chu M, et al. (2002). Positional cloning of the combined hyperlipidemia gene Hyplip1. *Nat. Genet* 30, 110–116. [PubMed: 11753387]
- Chutkow WA, Patwari P, Yoshioka J, and Lee RT (2008). Thioredoxin-interacting protein (Txnip) is a critical regulator of hepatic glucose production. *J. Biol. Chem* 283, 2397–2406. [PubMed: 17998203]
- Chutkow WA, Birkenfeld AL, Brown JD, Lee HY, Frederick DW, Yoshioka J, Patwari P, Kursawe R, Cushman SW, Plutzky J, et al. (2010). Deletion of the alpha-arrestin protein Txnip in mice promotes adiposity and adipogenesis while preserving insulin sensitivity. *Diabetes* 59, 1424–1434. [PubMed: 20299477]
- Dobin A, Davis CA, Schlesinger F, Drenkow J, Zaleski C, Jha S, Batut P, Chaisson M, and Gingeras TR (2013). STAR: ultrafast universal RNA-seq aligner. *Bioinformatics* 29, 15–21. [PubMed: 23104886]
- Eguchi J, Wang X, Yu S, Kershaw EE, Chiu PC, Dushay J, Estall JL, Klein U, Maratos-Flier E, and Rosen ED (2011). Transcriptional control of adipose lipid handling by IRF4. *Cell Metab* 13, 249–259. [PubMed: 21356515]
- Gu Z, Eils R, and Schlesner M (2016). Complex heatmaps reveal patterns and correlations in multidimensional genomic data. *Bioinformatics* 32, 2847–2849. [PubMed: 27207943]
- Han X, Yang K, Yang J, Cheng H, and Gross RW (2006). Shotgun lipidomics of cardiolipin molecular species in lipid extracts of biological samples. *J. Lipid Res* 47, 864–879. [PubMed: 16449763]
- Harris FM, Best KB, and Bell JD (2002). Use of laurdan fluorescence intensity and polarization to distinguish changes in membrane fluidity and phospholipid order. *Biochim. Biophys. Acta* 1565, 123–128. [PubMed: 12225860]
- Hoang T, Smith MD, and Jelokhani-Niaraki M (2013). Expression, folding, and proton transport activity of human uncoupling protein-1 (UCP1) in lipid membranes: evidence for associated functional forms. *J. Biol. Chem* 288, 36244–36258. [PubMed: 24196960]
- Hui TY, Sheth SS, Diffley JM, Potter DW, Lusic AJ, Attie AD, and Davis RA (2004). Mice lacking thioredoxin-interacting protein provide evidence linking cellular redox state to appropriate response to nutritional signals. *J. Biol. Chem* 279, 24387–24393. [PubMed: 15047687]
- Ikon N, and Ryan RO (2017). Cardiolipin and mitochondrial cristae organization. *Biochim. Biophys. Acta Biomembr* 1859, 1156–1163. [PubMed: 28336315]
- Indiveri C, Iacobazzi V, Tonazzi A, Giangregorio N, Infantino V, Convertini P, Console L, and Palmieri F (2011). The mitochondrial carnitine/acyl-carnitine carrier: function, structure and physiopathology. *Mol. Aspects Med* 32, 223–233. [PubMed: 22020112]
- Jørgensen JA, Zadravec D, and Jacobsson A (2007). Norepinephrine and rosiglitazone synergistically induce Elovl3 expression in brown adipocytes. *Am. J. Physiol. Endocrinol. Metab* 293, E1159–E1168. [PubMed: 17726147]
- Karsai G, Lone M, Kutalik Z, Brenna JT, Li H, Pan D, von Eckardstein A, and Hornemann T (2020). FADS3 is a 14Z sphingoid base desaturase that contributes to gender differences in the human plasma sphingolipidome. *J. Biol. Chem* 295, 1889–1897. [PubMed: 31862735]
- Lefterova MI, Zhang Y, Steger DJ, Schupp M, Schug J, Cristancho A, Feng D, Zhuo D, Stoeckert CJ Jr., Liu XS, and Lazar MA (2008). PPARgamma and C/EBP factors orchestrate adipocyte biology via adjacent binding on a genome-wide scale. *Genes Dev* 22, 2941–2952. [PubMed: 18981473]
- Lerner AG, Upton JP, Praveen PV, Ghosh R, Nakagawa Y, Igbaria A, Shen S, Nguyen V, Backes BJ, Heiman M, et al. (2012). IRE1 $\alpha$  induces thioredoxin-interacting protein to activate the NLRP3 inflammasome and promote programmed cell death under irremediable ER stress. *Cell Metab* 16, 250–264. [PubMed: 22883233]
- Liao Y, Smyth GK, and Shi W (2014). featureCounts: an efficient general purpose program for assigning sequence reads to genomic features. *Bioinformatics* 30, 923–930. [PubMed: 24227677]
- Love MI, Huber W, and Anders S (2014). Moderated estimation of fold change and dispersion for RNA-seq data with DESeq2. *Genome Biol* 15, 550. [PubMed: 25516281]

- McCommis KS, and Finck BN (2015). Mitochondrial pyruvate transport: a historical perspective and future research directions. *Biochem. J* 466, 443–454. [PubMed: 25748677]
- Miyamoto J, Ohue-Kitano R, Mukoyama H, Nishida A, Watanabe K, Igarashi M, Irie J, Tsujimoto G, Satoh-Asahara N, Itoh H, and Kimura I (2019). Ketone body receptor GPR43 regulates lipid metabolism under ketogenic conditions. *Proc. Natl. Acad. Sci. USA* 116, 23813–23821. [PubMed: 31685604]
- Mráček T, Drahoš Z, and Houšťková J (2013). The function and the role of the mitochondrial glycerol-3-phosphate dehydrogenase in mammalian tissues. *Biochim. Biophys. Acta* 1827, 401–410. [PubMed: 23220394]
- Nguyen LN, Ma D, Shui G, Wong P, Cazenave-Gassiot A, Zhang X, Wenk MR, Goh EL, and Silver DL (2014). Mfsd2a is a transporter for the essential omega-3 fatty acid docosahexaenoic acid. *Nature* 509, 503–506. [PubMed: 24828044]
- Ohno Y, Suto S, Yamanaka M, Mizutani Y, Mitsutake S, Igarashi Y, Sassa T, and Kihara A (2010). ELOVL1 production of C24 acyl-CoAs is linked to C24 sphingolipid synthesis. *Proc. Natl. Acad. Sci. USA* 107, 18439–18444. [PubMed: 20937905]
- Osłowski CM, Hara T, O’Sullivan-Murphy B, Kanekura K, Lu S, Hara M, Ishigaki S, Zhu LJ, Hayashi E, Hui ST, et al. (2012). Thioredoxin-interacting protein mediates ER stress-induced  $\beta$  cell death through initiation of the inflammasome. *Cell Metab* 16, 265–273. [PubMed: 22883234]
- Parasassi T, De Stasio G, Ravagnan G, Rusch RM, and Gratton E (1991). Quantitation of lipid phases in phospholipid vesicles by the generalized polarization of Laurdan fluorescence. *Biophys. J* 60, 179–189. [PubMed: 1883937]
- Parikh H, Carlsson E, Chutkow WA, Johansson LE, Storgaard H, Poulsen P, Saxena R, Ladd C, Schulze PC, Mazzini MJ, et al. (2007). TXNIP regulates peripheral glucose metabolism in humans. *PLoS Med* 4, e158. [PubMed: 17472435]
- Puigserver P, Wu Z, Park CW, Graves R, Wright M, and Spiegelman BM (1998). A cold-inducible coactivator of nuclear receptors linked to adaptive thermogenesis. *Cell* 92, 829–839. [PubMed: 9529258]
- Rioux V, Pédrone F, Blanchard H, Duby C, Boulier-Monthéan N, Bernard L, Beauchamp E, Catheline D, and Legrand P (2013). Trans-vaccenate is  $\Delta^{13}$ -desaturated by FADS3 in rodents. *J. Lipid Res* 54, 3438–3452. [PubMed: 24070791]
- Röhrig F, and Schulze A (2016). The multifaceted roles of fatty acid synthesis in cancer. *Nat. Rev. Cancer* 16, 732–749. [PubMed: 27658529]
- Rutkowski DT (2019). Liver function and dysfunction - a unique window into the physiological reach of ER stress and the unfolded protein response. *FEBS J* 286, 356–378. [PubMed: 29360258]
- Schroeder F, and Goh EH (1980). Effect of fatty acids on physical properties of microsomes from isolated perfused rat liver. *Chem. Phys. Lipids* 26, 207–224. [PubMed: 7371116]
- Sheth SS, Castellani LW, Chari S, Wagg C, Thippavong CK, Bodnar JS, Tontonoz P, Attie AD, Lopaschuk GD, and Lusis AJ (2005). Thioredoxin-interacting protein deficiency disrupts the fasting-feeding metabolic transition. *J. Lipid Res* 46, 123–134. [PubMed: 15520447]
- Shimazu T, Hirschey MD, Newman J, He W, Shirakawa K, Le Moan N, Grueter CA, Lim H, Saunders LR, Stevens RD, et al. (2013). Suppression of oxidative stress by  $\beta$ -hydroxybutyrate, an endogenous histone deacetylase inhibitor. *Science* 339, 211–214. [PubMed: 23223453]
- Smithson M, and Verkuilen J (2006). A better lemon squeezer? Maximum-likelihood regression with beta-distributed dependent variables. *Psychol. Methods* 11, 54–71. [PubMed: 16594767]
- Stoltzman CA, Peterson CW, Breen KT, Muoio DM, Billin AN, and Ayer DE (2008). Glucose sensing by MondoA:MLX complexes: a role for hexokinases and direct regulation of thioredoxin-interacting protein expression. *Proc. Natl. Acad. Sci. USA* 105, 6912–6917. [PubMed: 18458340]
- Subramanian A, Tamayo P, Mootha VK, Mukherjee S, Ebert BL, Gillette MA, Paulovich A, Pomeroy SL, Golub TR, Lander ES, and Mesirov JP (2005). Gene set enrichment analysis: a knowledge-based approach for interpreting genome-wide expression profiles. *Proc. Natl. Acad. Sci. USA* 102, 15545–15550. [PubMed: 16199517]
- Sustarsic EG, Ma T, Lynes MD, Larsen M, Karavaeva I, Havelund JF, Nielsen CH, Jedrychowski MP, Moreno-Torres M, Lundh M, et al. (2018). Cardiolipin Synthesis in Brown and Beige

- Fat Mitochondria Is Essential for Systemic Energy Homeostasis. *Cell Metab* 28, 159–174.e11. [PubMed: 29861389]
- Uyeda K, Yamashita H, and Kawaguchi T (2002). Carbohydrate responsive element-binding protein (ChREBP): a key regulator of glucose metabolism and fat storage. *Biochem. Pharmacol* 63, 2075–2080. [PubMed: 12110366]
- Villarroya F, Iglesias R, and Giralt M (2007). PPARs in the Control of Uncoupling Proteins Gene Expression. *PPAR Res* 2007, 74364. [PubMed: 17389766]
- Waldhart AN, Dykstra H, Peck AS, Boguslawski EA, Madaj ZB, Wen J, Veldkamp K, Hollowell M, Zheng B, Cantley LC, et al. (2017). Phosphorylation of TXNIP by AKT Mediates Acute Influx of Glucose in Response to Insulin. *Cell Rep* 19, 2005–2013. [PubMed: 28591573]
- Wang M, and Han X (2014). Multidimensional mass spectrometry-based shotgun lipidomics. *Methods Mol. Biol* 1198, 203–220. [PubMed: 25270931]
- Wong BH, Chan JP, Cazenave-Gassiot A, Poh RW, Foo JC, Galam DL, Ghosh S, Nguyen LN, Barathi VA, Yeo SW, et al. (2016). Mfsd2a Is a Transporter for the Essential  $\omega$ -3 Fatty Acid Docosahexaenoic Acid (DHA) in Eye and Is Important for Photoreceptor Cell Development. *J. Biol. Chem* 291, 10501–10514. [PubMed: 27008858]
- Wu N, Zheng B, Shaywitz A, Dagon Y, Tower C, Bellinger G, Shen CH, Wen J, Asara J, McGraw TE, et al. (2013). AMPK-dependent degradation of TXNIP upon energy stress leads to enhanced glucose uptake via GLUT1. *Mol. Cell* 49, 1167–1175. [PubMed: 23453806]
- Yu G, Wang LG, Han Y, and He QY (2012). clusterProfiler: an R package for comparing biological themes among gene clusters. *OMICS* 16, 284–287. [PubMed: 22455463]
- Zhou R, Tardivel A, Thorens B, Choi I, and Tschopp J (2010). Thioredoxin-interacting protein links oxidative stress to inflammasome activation. *Nat. Immunol* 11, 136–140. [PubMed: 20023662]

### Highlights

- TXNIP knockout effectively reduces the concentration of dietary PUFA in tissues
- Excess glucose reduces the expression of genes involved in fatty acid elongation
- Reduced PUFA content affects BAT mitochondria function under cold stress

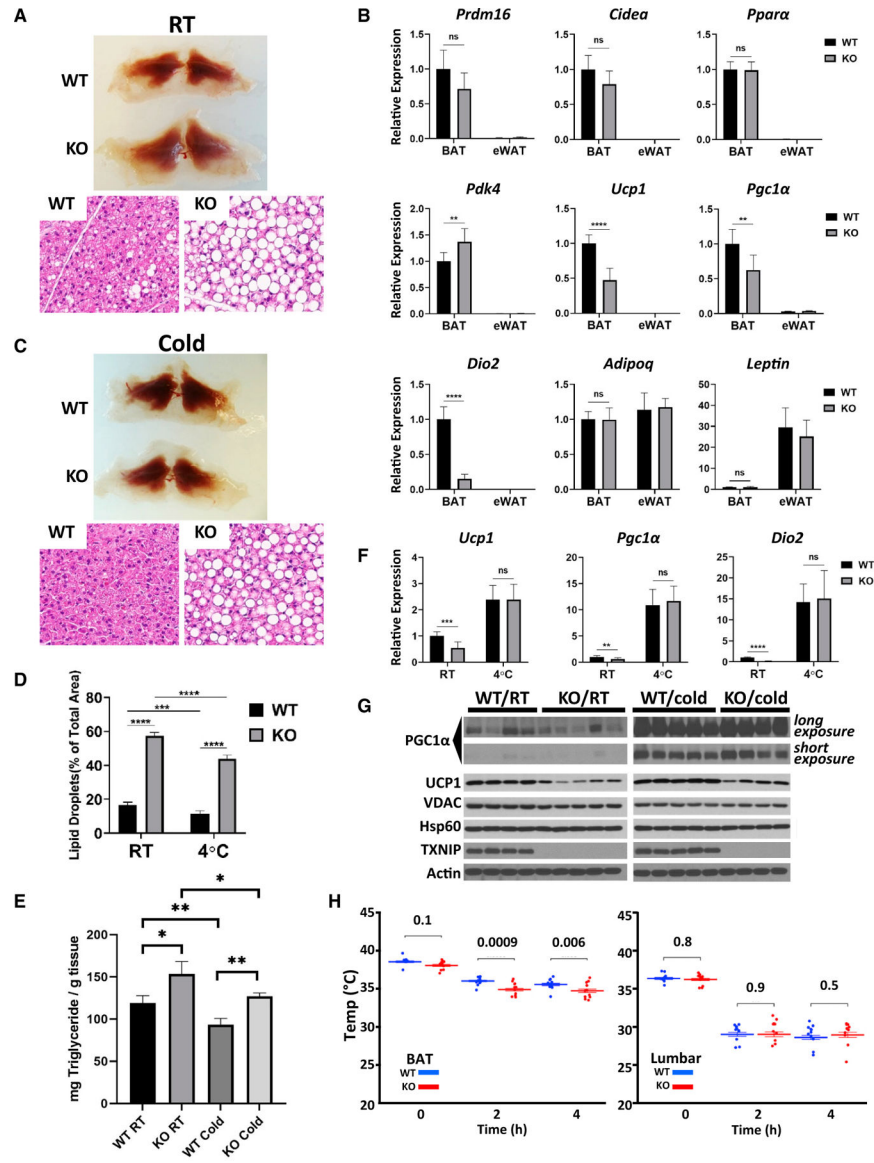


**Figure 1. TXNIP KO BAT has defects in thermogenesis**

(A) BAT morphology, H&E stain at RT.

(B) BAT and eWAT gene expression at RT by qPCR (n = 7).

(C) BAT morphology and H&E stain after 4-h cold stress.

(D) Quantitation of lipid droplets from BAT H&E slides.

(E) Quantitation of TAG content in BAT.

(F) BAT gene expression by qPCR (n = 7).

(G) BAT western blot.

(H) Intrascapular and lumbar temperature during cold stress (n = 10).

For gene expression and lipid quantification, error bars show the mean  $\pm$  SD; \*p < 0.05; \*\*p < 0.01; \*\*\*p < 0.001; \*\*\*\*p < 0.0001 (Student's t test, unpaired, two-tailed).

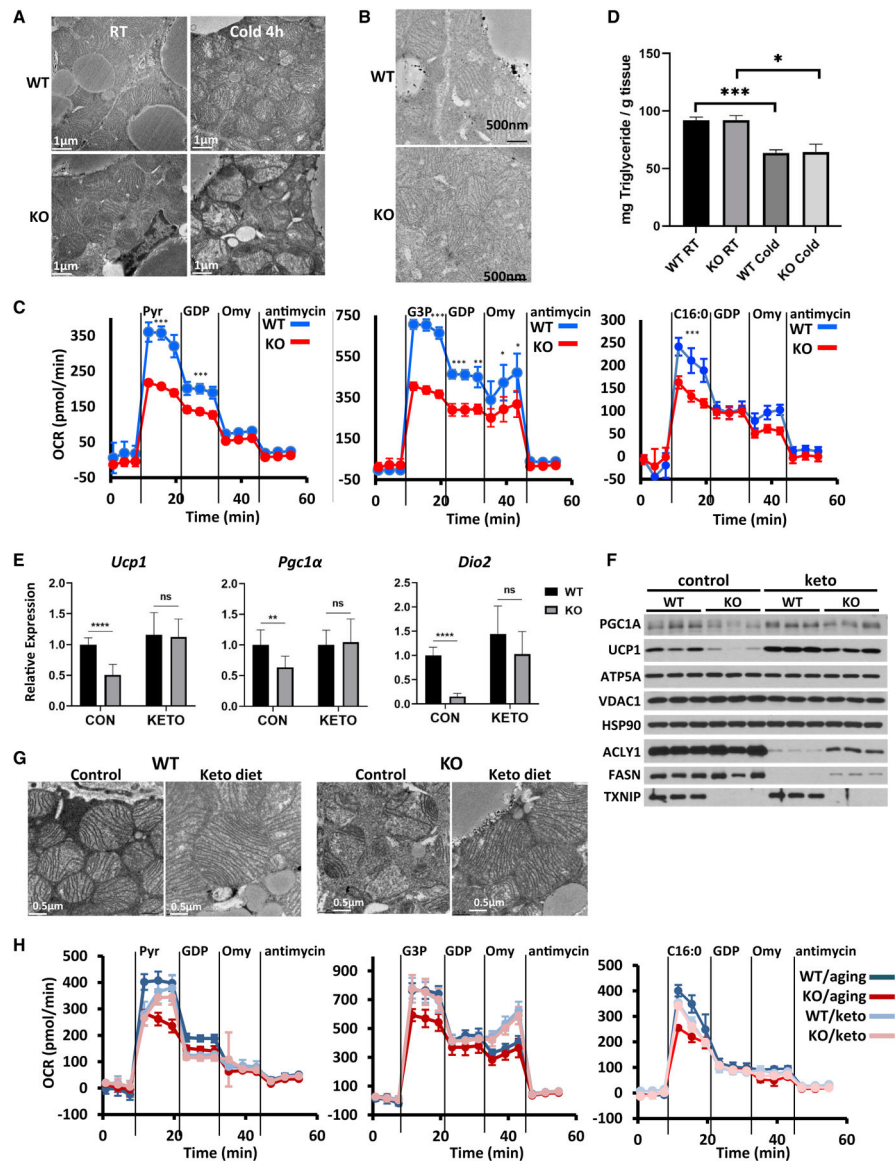


**Figure 2. TXNIP KO BAT mitochondria functional defects rescued by a ketogenic diet**  
 (A) BAT TEM, before and after 4 h of cold stress.  
 (B) BAT TEM, after a 4 h cold stress followed by 4 h recovery at RT.  
 (C) Representative Seahorse OCR of isolated mitochondria from BAT after 4 h of cold stress.  
 (D) Quantification of TAG in BAT on ketogenic diet.  
 (E) *Ucp1*, *Pgc1α*, and *Dio2* expression levels in BAT on different diets at RT by qPCR.  
 (F) Western blot of BAT on different diets at RT.  
 (G) BAT TEM on different diets after 4 h of cold stress.  
 (H) Seahorse OCR measured as in (C) from animals on ketogenic diet.

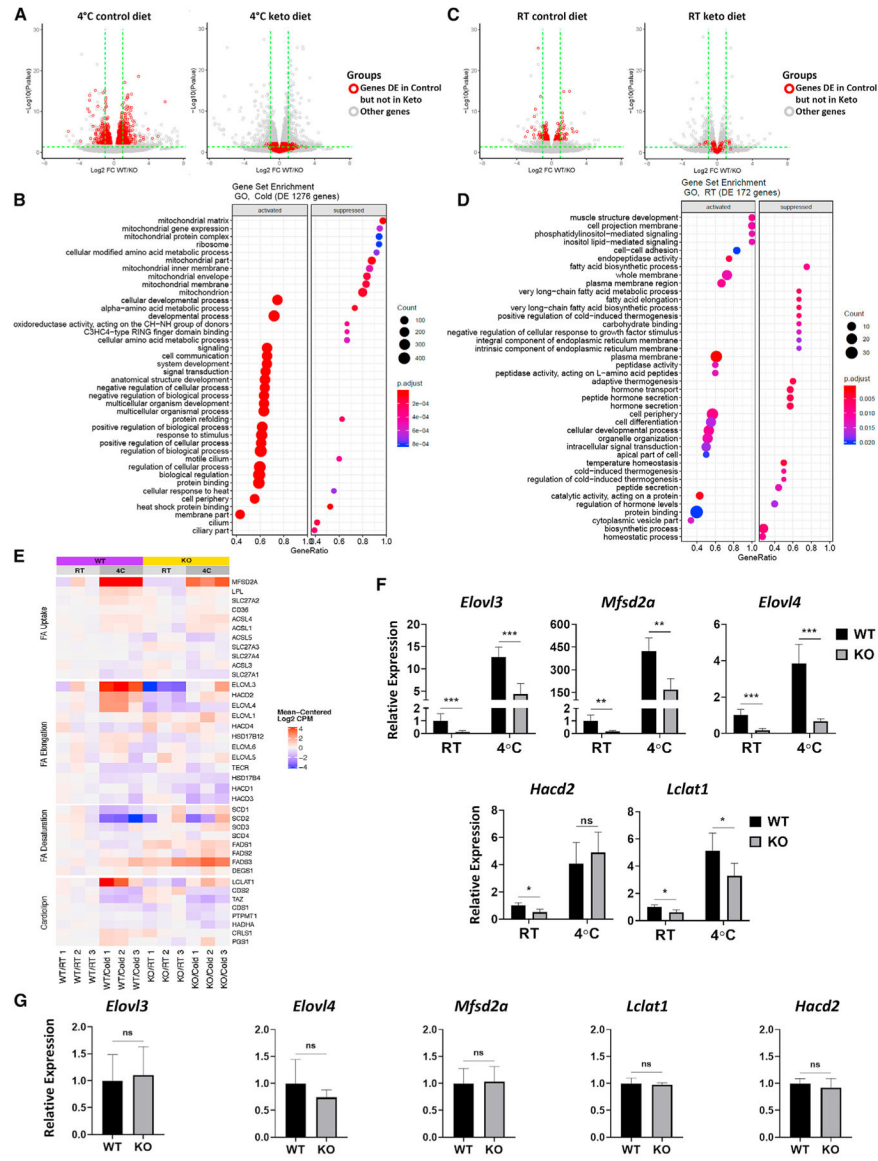


**Figure 3. TXNIP KO BAT has lower expression of genes in PUFA transport and elongation** (A) Volcano plot showing genome-wide transcriptional changes between TXNIP WT and KO BAT after 4 h of cold stress for the control diet (left) and a ketogenic diet (right). Red dots represent genes with significant differential expression (FDR <0.05) between WT and KO on the control diet but not on the ketogenic diet (FDR = 0.05). All other genes are represented by gray dots. The horizontal dashed line indicates the p value 0.05, while the vertical demarcates twice up- or downregulated genes. (B) GO-based gene set enrichment for genes having significant differential expression between TXNIP WT and KO on the control but not the ketogenic diet after a 4-h cold stress. Gene ratio (horizontal axis) is M/N where M = number of genes in our gene list in a given pathway, N = number of predefined unique genes in the same pathway. (C) The same as (A) for RT. (D) The same as (B) for RT.

(E) Gene expression in fatty acid uptake, elongation, desaturation, and cardioliipin synthesis and remodeling pathways from mRNA-seq data on control diet.

(F) qPCR verification of selected gene expression from the heatmap (n = 7).

(G) qPCR verification of gene expression on the ketogenic diet at RT (n = 7). For gene expression, error bars show mean  $\pm$  SD; \*p < 0.05; \*\*p < 0.01; \*\*\*p < 0.001 (Student's t test).

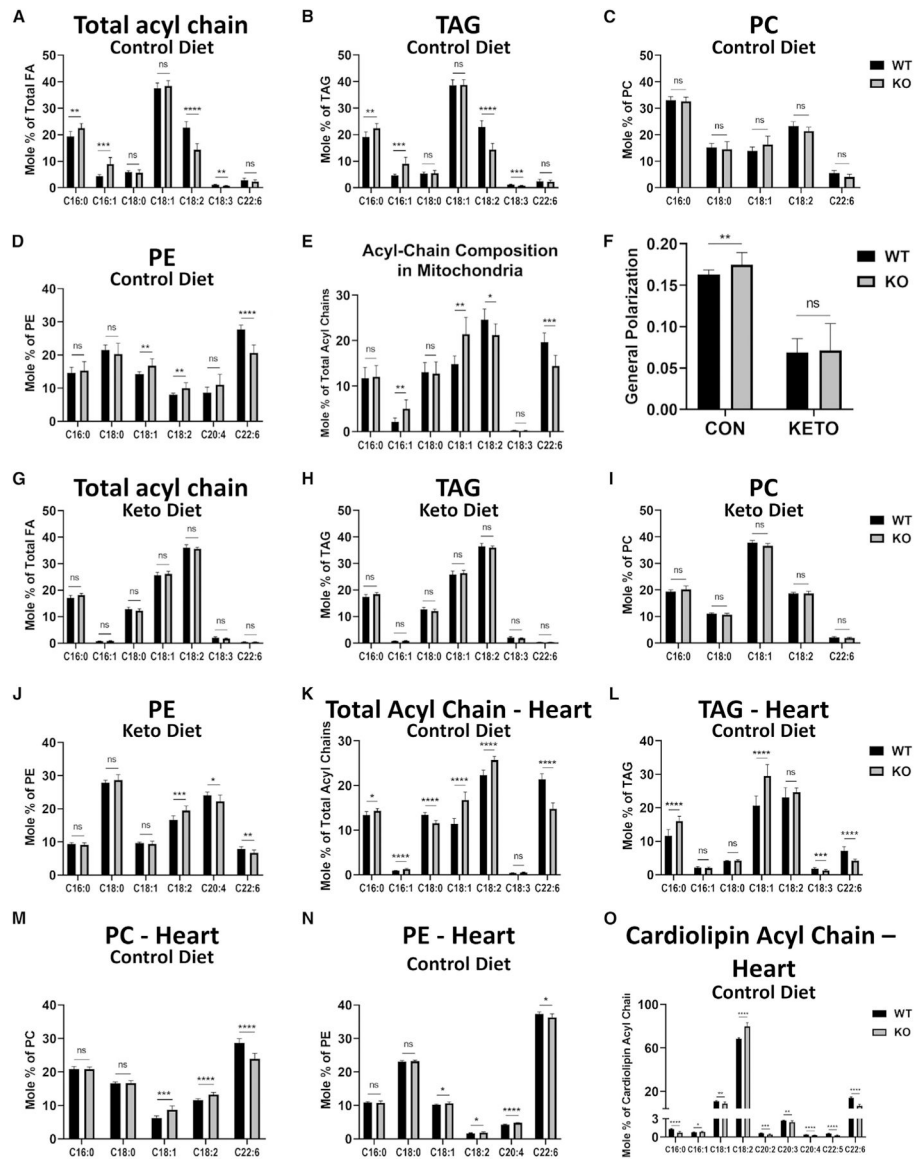


**Figure 4. Lipidomics analysis of BAT showing less PUFA in KO (n = 8, males)**  
 (A–E) Total fatty acid acyl-chain species (A), acyl-chain composition of TAG (B), PC (C), and PE (D), and total acyl-chain (E) of isolated mitochondria from BAT of TXNIP WT and KO animals at RT on control diet. Only the most abundant species are shown for clarity.  
 (F) Membrane fluidity measured as Laurdan general polarization in isolated mitochondria from WT and KO on the control and ketogenic diet.  
 (G–J) Total acyl-chain species (G), acyl-chain composition of TAG (H), PC (I), and PE (J) of WT and KO BAT on a ketogenic diet.  
 (K–O) Total acyl-chain (K), acyl-chain composition of TAG (L), PC (M), PE (N), and cardiolipin (O) of WT and KO heart on the control diet. \* $p = 0.01 < p < 0.05$ ; \*\* $p = 0.001 < p < 0.01$ ; \*\*\* $p < 0.001$

## KEY RESOURCES TABLE

Reagent or resource	Source	Identifier
Antibodies		
PGC1 $\alpha$	Millipore	ST1203; RRID: AB_10806332
UCP1	R&D	MAB6158; RRID: AB_10572490
VDAC	Cell Signaling Tech.	4866; RRID: AB_2272627
Hsp60	Cell Signaling Tech.	12165; RRID: AB_2636980
TXNIP	Cell Signaling Tech.	14715; RRID: AB_2714178
actin	Sigma	A4700; RRID: AB_476730
ATP5A	Abcam	ab176569; RRID: AB_2801536
Hsp90	Santa Cruz Biotech	sc13119; RRID: AB_675659
ACLY1	Cell Signaling Tech.	13390; RRID: AB_2798203
FASN	Cell Signaling Tech.	3180; RRID: AB_2100796
Critical commercial assays		
Ketone body Assay kit	Cayman Chemical	700190
Infinity Triglyceride kit	ThermoFisher Scientific	TR22421
Deposited data		
mRNaseq on control diet	BioProject	PRJNA573103
mRNaseq on ketogenic diet	BioProject	PRJNA681590
Experimental models: Organisms/strains		
B6;129- <i>Txnip</i> <sup>tm1Rlee/J</sup>	JAX 016847	TXNIP <sup>fl/fl</sup>
B6.C-Tg(CMV-cre)1Cgn/J	JAX 006054	CMV-cre
B6.FVB-Tg(Adipoq-cre)1Evdrr/J	JAX 028020	Adipoq-cre
Oligonucleotides		
See Table S3		N/A
Software and algorithms		
SnakePipes	(Bhardwaj et al., 2019)	<a href="https://snakepipes.readthedocs.io/en/latest/">https://snakepipes.readthedocs.io/en/latest/</a>
STAR aligner	(Dobin et al., 2013)	<a href="https://github.com/alexdobin/STAR/releases">https://github.com/alexdobin/STAR/releases</a>
FeatureCounts	(Liao et al., 2014)	<a href="http://bioinf.wehi.edu.au/featureCounts/">http://bioinf.wehi.edu.au/featureCounts/</a>
DESeq2	(Love et al., 2014)	<a href="https://bioconductor.org/packages/release/bioc/html/DESeq2.html">https://bioconductor.org/packages/release/bioc/html/DESeq2.html</a>
ComplexHeatmap R package	(Gu et al., 2016)	<a href="https://bioconductor.org/packages/release/bioc/html/ComplexHeatmap.html">https://bioconductor.org/packages/release/bioc/html/ComplexHeatmap.html</a>
ClusterProfiler R package	(Subramanian et al., 2005; Yu et al., 2012)	<a href="https://bioconductor.org/packages/release/bioc/html/clusterProfiler.html">https://bioconductor.org/packages/release/bioc/html/clusterProfiler.html</a>